Received: 8 October 2016 | Revised: 31 July 2017 | Accepted: 14 August 2017

DOI: 10.1002/nbm.3805

WILEY NMR IN BIOMEDICINE

SPECIAL ISSUE REVIEW ARTICLE

Advances in computational and statistical diffusion MRI

Lauren J. O'Donnell[1] | **Alessandro Daducci**[2,3] | **Demian Wassermann**[4] | **Christophe Lenglet**[5]

[1]Brigham and Women's Hospital and Harvard Medical School, Boston, MA, USA
[2]Computer Science department, University of Verona, Verona, Italy
[3]Radiology department, Centre Hospitalier Universitaire Vaudois (CHUV), Lausanne, Switzerland
[4]Athena Team, Inria Sophia Antipolis-Méditerranée, 2004 route des Lucioles 06902 Biot, France
[5]Center for Magnetic Resonance Research, University of Minnesota, Minneapolis, MN, USA

Correspondence
Lauren J. O'Donnell, Brigham and Women's Hospital and Harvard Medical School, Boston, MA, USA.
Email: odonnell@bwh.harvard.edu

Funding information
NIH P41 EB015894, R01 EB008432, U01 CA199459, R03 NS088301, P41 EB015898, P41 EB015902 and R01 MH074794; Center for Biomedical Imaging (CIBM); Geneva-Lausanne Universities and the EPFL

Computational methods are crucial for the analysis of diffusion magnetic resonance imaging (MRI) of the brain. Computational diffusion MRI can provide rich information at many size scales, including local microstructure measures such as diffusion anisotropies or apparent axon diameters, whole-brain connectivity information that describes the brain's wiring diagram and population-based studies in health and disease. Many of the diffusion MRI analyses performed today were not possible five, ten or twenty years ago, due to the requirements for large amounts of computer memory or processor time. In addition, mathematical frameworks had to be developed or adapted from other fields to create new ways to analyze diffusion MRI data. The purpose of this review is to highlight recent computational and statistical advances in diffusion MRI and to put these advances into context by comparison with the more traditional computational methods that are in popular clinical and scientific use. We aim to provide a high-level overview of interest to diffusion MRI researchers, with a more in-depth treatment to illustrate selected computational advances.

KEYWORDS
diffusion MRI, registration, statistics, tractography

1 | INTRODUCTION

By measuring the diffusion of water molecules that probe the brain's microstructure at the cellular scale, diffusion magnetic resonance imaging (dMRI) provides unique information about the living human brain in health and disease.[1,2] Unlike traditional structural MRI acquisitions that provide scalar maps directly (such as T_1, T_2, or susceptibility-weighted images), dMRI acquisitions require multiple measurements to assess brain microstructure and connectivity. Current dMRI protocols produce from seven to hundreds of diffusion-weighted measurements, which are acquired at different orientations and often using different amounts of diffusion weighting. Due to the complex nature of these data, computational analysis methods are essential to produce advanced visualization or quantitation (Figure 1). In the application of dMRI to the study of brain microstructure and connectivity, computational analyses can be performed at multiple neuroanatomical scales, ranging from the microstructure scale of diffusion compartments to the voxel scale of local white or gray matter anatomy, the whole-brain scale of connections estimated using tractography and finally the population scale for neuroscientific studies.[3-8] Note, though, that there is an important mismatch of size scales between white matter neurons and much larger dMRI measurement voxels.[9] Many mathematical modeling approaches have tried to bridge this gap.

Since the introduction of the diffusion tensor model in [15] computational methods for dMRI have become an increasingly active area of research. Techniques initially developed for scalar medical images, such as registration, segmentation and statistical analyses, have been extended and adapted to various forms of dMRI data, including voxel-level and tract-level data representations. dMRI has enabled one unique computational analysis method, tractography, which is the process of tracing the brain's white matter connections (fiber tracts) non-invasively. Many of the

Abbreviations used: COMMIT, Convex Optimization Modeling for Microstructure Informed Tractography; CSD, constrained spherical deconvolution; dMRI, diffusion magnetic resonance imaging; DSI, diffusion spectrum imaging; DT, diffusion tensor; DTI, diffusion tensor imaging; DWI, diffusion-weighted image; fODF, fiber orientation distribution function; GA, geodesic anisotropy; HARDI, high angular resolution diffusion imaging; LiFE, Linear Fascicle Evaluation; ODF, orientation distribution function; PPD, preservation of principal direction; SIFT, Spherical-deconvolution Informed Filtering of Tractograms

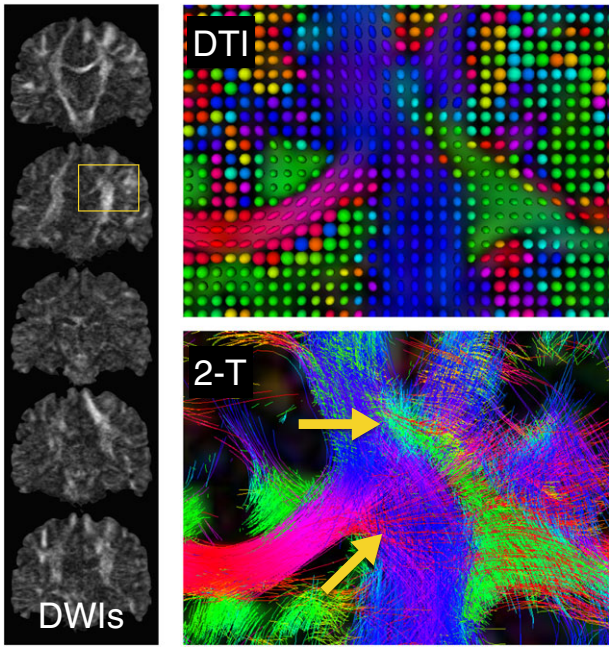

FIGURE 1 Computational methods for diffusion MRI are needed to analyze input diffusion-weighted image (DWI) data to enable visualization or quantitation. At the left, coronal images show DWIs acquired using several gradient directions. The yellow box indicates the zoomed region shown in the images at the right, which result from computational analysis of the DWIs. Colors encode fiber orientation such that left–right is red, inferior–superior is blue, and anterior–posterior is green. The traditional single diffusion tensor model (DTI, top right) is shown using ellipsoids for tensor visualization. DTI analysis has led to important findings, but it cannot represent anatomical fiber tract crossings (bottom right image, arrows), which can be seen with a multi-fiber model such as the two-tensor (2-T)[10,11] tractography shown here. These images were created using the first dataset from the Human Connectome Project[12] using the SlicerDMRI package in 3D Slicer[13,14]

computational dMRI studies performed today were not possible five, ten or twenty years ago: many analyses require large amounts of memory and long processor times, or had high computational complexity and required optimization to become feasible. In some cases (see Section 3), mathematical frameworks had to be developed or adapted from other fields (e.g. statistics or geometry) to create new ways to analyze dMRI data.

In this review, we will focus on the historical evolution and recent advances in three selected computational analyses of dMRI: tractography, statistical analysis and registration (dMRI tract-based segmentation was recently reviewed).[16] We will begin this review at the whole-brain scale, with tractography (Section 2), which is commonly performed in individual subject data. Next we will give an overview of the mathematics of statistical analysis of local diffusion models (Section 3), which are generally analyzed in groups of subjects. Finally, we will discuss how different representations of dMRI data, both tractography and voxel-level diffusion information, can be used for registration (Section 4), which is most often employed across subjects. Where possible, we will contrast standard dMRI computational methods with more advanced ones to show when the latter might be useful, with consideration of the potential differences in computational cost. Finally, we will conclude with an overall look at future directions for computational diffusion MRI.

2 | WHITE MATTER TRACTOGRAPHY: A COMPUTATIONAL PERSPECTIVE

Tractography, the process of inferring white matter pathways from dMRI data, is an invaluable tool for studying the brain's structural connectivity non-invasively.[17,18] Despite the large number of available methods (see Jeurissen et al.[19] for a comprehensive review), the reconstructed pathways are not truly quantitative and reflect the actual white matter structure only indirectly.[20,21] In this section, we describe selected computational advances that represented major steps forward in terms of accuracy and interpretation of connectivity estimates (Figure 2). All reported benchmarks are intended as indicative values of the algorithms (as described in the original publications) for a typical dataset size and a standard workstation, without using multi-threading or parallel computing, unless otherwise specified.

2.1 | Tractography as line propagation

Tractography was originally formulated as a *line-propagation problem*:

$$\frac{d\mathbf{f}(s)}{ds} = \mathbf{v}(\mathbf{f}(s)) \text{ with } \begin{cases} 0 \le s \le 1 \\ \mathbf{f}(0) = \mathbf{f}_0 \end{cases} \quad (1)$$

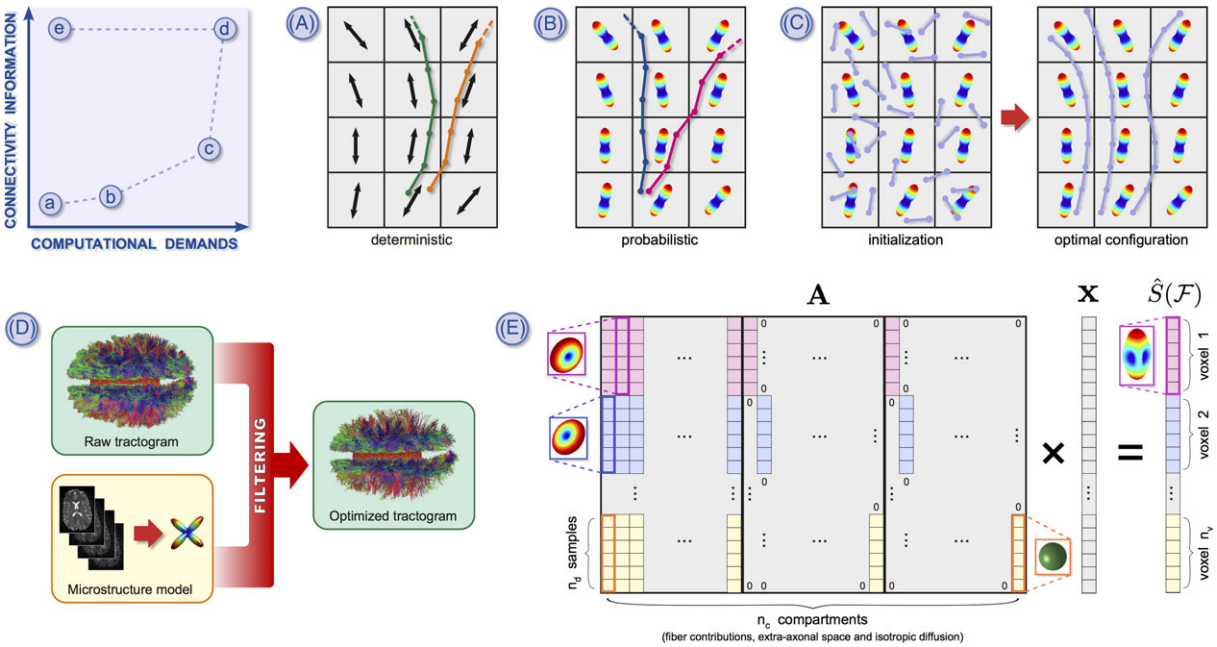

FIGURE 2 Computational demands and benefits for quantifying the connectivity of notable formulations proposed to date for tractography: *line propagation* (A, deterministic; B, probabilistic), *global inverse problem* (C, bottom-up), and *microstructure informed tractography* (D, top-down; E, dictionary-based)

where a streamline $\mathbf{f}$, parameterized by arc-length s, is constructed iteratively from a starting point $\mathbf{f}_0 \in \mathbb{R}^3$ following the principal diffusion direction $\mathbf{v}$ estimated along the path with DTI.[22,23] This *deterministic* procedure (Figure 2A) is very fast (a few minutes per subject), but also extremely sensitive to local inaccuracies in estimating the propagation direction; moreover, the reconstructed streamlines do not provide a direct means of quantifying the underlying connectivity.[20,24] In *probabilistic* methods,[25,26] the propagation direction is sampled from a distribution estimated from advanced diffusion models (Figure 2B) and probability maps are created by generating a high number of streamlines from each seed location. This tracking strategy is computationally expensive ($\approx$ 1 day per subject) and may not improve the estimation of connectivity substantially, as these probabilities are difficult to interpret and have often been mistakenly considered as anatomical connection strengths.[20]

2.2 | Tractography as an inverse problem

Recent approaches have directly acknowledged the ill-posed nature of tractography and tackled the reconstruction as a *global inverse problem* (Figure 2C–E):

$$\mathcal{F} = \text{argmax}\ \mathcal{E}\left(S, \hat{S}(\mathcal{F})\right) \tag{2}$$

in which the set of streamlines $\mathcal{F}$, also known as the tractogram, that maximizes the similarity $\mathcal{E}(\cdot,\cdot)$ between the acquired diffusion MR images, S, and those predicted from $\mathcal{F}$, $\hat{S}(\mathcal{F})$, is estimated simultaneously using global optimization.

Bottom-up methods[27,28] construct the tractogram starting from an initial set of fixed-length segments, where each segment contributes to the predicted signal according to a tensor-based generative model and the optimization encourages segments to concatenate into long chains while fitting the measured data (Figure 2C). While reconstructions showed an unparalleled level of detail, the tracking process became computationally impractical ($\approx$ 1 month per subject). The model was later simplified by Reisert et al.,[29] who decreased the processing time significantly to a few hours per subject. Sherbondy et al.[30] approached the reconstruction problem in a *top-down* fashion (Figure 2D). The BlueMatter algorithm built a massive collection of candidate streamlines ($\approx$ 180 billion) combining the output from different tractography algorithms and used a stochastic search to determine the optimal subset that best explained the acquired dMRI data. Although it required nine days on a 2048-core supercomputer with 500 GB of memory, BlueMatter offered a novel solution to tackle tractography from a different angle, opening new perspectives for the quantification of connectivity.

Spherical-deconvolution Informed Filtering of Tractograms (SIFT)[31] followed the same *pruning strategy*, but cut computational demands down to $\approx$ 15 – 20 hours per subject on standard workstations using an efficient heuristic to approximate the similarity $\mathcal{E}$. SIFT selectively removes streamlines guided by the fiber orientation distribution function (fODF) estimated in each voxel with constrained spherical deconvolution (CSD);[32] however, the procedure requires a very large number of initial candidates ($\approx$ 100 million) and a considerable amount of memory ($\approx$ 26 GB per subject). In SIFT2,[33] rather than discarding streamlines, the algorithm attempts to estimate their 'effective volume' using a CSD-based generative model and assigning a cross-sectional area to each. This approach needs a lower number of candidates ($\approx$ 10 million) and improves both

computation time (a few hours per subject) and memory consumption (a few GB per subject). Recent studies showed that tractograms optimized with these pruning techniques provide more robust and biologically meaningful estimates of the underlying connectivity.[34,35] Nevertheless, SIFT/SIFT2 use a similarity function based on the reconstructed fODFs rather than the full dMRI data and thus cannot exploit possible additional information about the microstructural composition of the fascicles, e.g. apparent axon caliber, which may improve quantification of connectivity further.

2.3 | Tractography with microstructure information

The integration of microstructure information into tractography represents the latest frontier in dMRI tractography. The first *microstructure-informed tractography* method was proposed by Sherbondy et al.,[36] who extended the pruning strategy of BlueMatter (Figure 2D) to allow simultaneous estimation of the optimal subset of fascicles and their biophysical parameters, invoking the assumption that these latter remain consistent along the fibers.* MicroTrack uses a biophysical model derived from Alexander et al.[37] to predict the diffusion MR images, $\hat{S}(\mathcal{F})$, and infer the effective volume and apparent average axon caliber of each fiber $\mathbf{f} \in \mathcal{F}$; specifically, the signal is expected to arise from water restricted inside the axons and hindered in the space around them, besides possible isotropic contributions from gray matter or cerebrospinal fluid. An efficient genetic algorithm enabled computation on standard workstations, but the processing time remained an issue (20 days per subject).

Malcolm et al.[10] approached the problem bottom-up and extended the line-propagation formulation of Equation 1 to take microstructure information into account in the integration process. At each tracking position, an unscented Kalman filter is used to simultaneously fit a multi-tensor model and determine the most consistent propagation direction using the information estimated at previous positions. Recent methods extended this idea by incorporating more advanced tissue microstructural models; Reddy and Rathi[38] built on the previous approach and used an enhanced version of the Neurite Orientation Dispersion Diffusion Imaging (NODDI) model[39] to deal with crossing fibers, whereas Girard et al.[40] used the Accelerated Cicrostructure Imaging Via Convex Optimization (AMICO) framework[41] to estimate, at each tracking position, the apparent mean axon caliber along the current tracking orientation. Being based on line propagation, these methods are considerably faster than MicroTrack (2 days per subject), but, at the same time, they also inherit all drawbacks of the local formulations described earlier.

These pioneering approaches served as a proof of concept for the great potential of tractography to benefit from microstructure information; however, despite encouraging preliminary results, the complexity of these initial solutions has hampered their widespread application in clinical research. A dramatic reduction in the computational burden was achieved with the *dictionary-based formulation* introduced by Daducci et al.,[42,43] (Figure 2E), who observed that the predicted signal from a tractogram $\mathcal{F}$, $\hat{S}(\mathcal{F})$, can be conveniently expressed in matrix form as

$$\hat{S}(\mathcal{F}) = \mathbf{A}\mathbf{x} \tag{3}$$

where $\mathbf{A} = \{a_{ij}\} \in \mathbb{R}^{n_v n_d \times n_c}$ is a linear operator mapping a multicompartment model analogous to MicroTrack to the n_d diffusion measurements in all n_v voxels. The contributions $\mathbf{x} \in \mathbb{R}^{n_c}_+$ of the corresponding n_c compartments, e.g. the fraction of restricted water inside the axons corresponding to fibers in $\mathcal{F}$, can be efficiently estimated using convex optimization:

$$\underset{\mathbf{x} \geq 0}{\operatorname{argmin}} \; \|\mathbf{A}\mathbf{x} - \mathbf{y}\|_2^2 \tag{4}$$

where $||\cdot||_2$ is the usual ℓ_2-norm in $\mathbb{R}^n$ and the cost function is the distance between the acquired diffusion MR images S, contained in the vector $\mathbf{y} \in \mathbb{R}^{n_d n_v}_+$, and those predicted from the tractogram $\mathcal{F}$ via the relation $\hat{S}(\mathcal{F}) = \mathbf{A}\mathbf{x}$.

This approach is named Convex Optimization Modeling for Microstructure Informed Tractography (COMMIT). COMMIT allows combination of tractography with virtually any diffusion model[44] and its convex formulation enables fast estimation (a few minutes per subject) that is guaranteed to converge to the optimal solution. Its memory usage is quite efficient (a few GB per subject): although $\mathbf{A}$ is extremely large, it is never stored explicitly and its columns are assembled at runtime, one at a time, using the Kronecker product and precomputed look-up tables. A similar mathematical formulation was recently implemented in Pestilli et al.,[45] but the Linear Fascicle Evaluation (LiFE) method was designed for validating the existence of fascicles rather than assessing their microstructure properties.

Microstructure-informed tractography is a relatively young but very promising area of research and these recent advances offer new and exciting possibilities for connectivity mapping, potentially opening the door to truly quantitative and biologically meaningful analyses of the brain's connectivity. Nonetheless, like any new technology, they also come with challenges and open questions (see Daducci et al.[46] for an extensive discussion), which are expected to stimulate research further.

3 | STATISTICS OF LOCAL DIFFUSION MODELS

Statistical analyses of neuroimaging data enable the quantitative study of the human brain in health and disease.[47,48] The mathematical characteristics of non-scalar entities derived from dMRI data, such as the diffusion tensor (DT) or orientation distribution function (ODF), have led to exciting

* Although this hypothesis might not be strictly true biologically, it is commonly accepted and actually used, implicitly or explicitly, in almost any tractography algorithm.

theoretical and computational developments. As mentioned in Section 4, defining a metric between these entities constitutes a key step to assess similarity, estimate distributions and test hypotheses that are critical for neuroscience[2] and clinical studies.[49] At the core of this line of research is the notion that the DT[1] and ODF[50-52] do not live in linear (Euclidean) spaces and therefore require appropriate theories to enforce physically meaningful properties, such as symmetry, positivity or integrability to 1, while avoiding potential statistical bias and significant increase in computational requirements. Compared with the computational costs of dMRI tractography or registration, the cost of statistical analyses often is lower and relates to the efficiency of metric computation.

The definition of differential geometrical structures for statistical models originated in 1936 with the work of Mahalanobis[53] for multivariate normal distributions with fixed covariance matrices. It was followed by Rao,[54] who showed that the Fisher information matrix could be used to define a Riemannian metric, therefore called the *Fisher–Rao* metric,[55] between parameterized probability density functions. Since then, the information geometry field[56,57] has provided a better understanding of those geometries and several articles have leveraged these concepts to develop statistical analysis methods for dMRI data. We hereby review some of the works that have addressed these questions.

3.1 | Diffusion tensors

Following a prior work where DTs were identified as elements of $\mathbb{R}^6$,[58] which ignores the algebraic properties of symmetric and positive-definite matrices, the concept of a tensor-variate normal distribution[59] was introduced to capture the variability of DTs via a symmetric positive-definite fourth-order tensor. Such approaches provided a convenient framework to estimate DT distributions and perform hypothesis testing, albeit not taking the geometry of DTs into account. This was achieved shortly after by modeling the space of DTs as a Riemannian symmetric space $GL^+(3)/SO(3)$, where $GL^+(3)$ is the set of real 3×3 matrices with positive determinant and $SO(3)$ is the set of real 3×3 orthogonal matrices with determinant 1.[60] In this pioneering work, the authors established methods and provided algorithms to compute statistics and modes of variations for DTs, using a metric that is naturally invariant under transformations from $GL^+(3)$. Subsequently, Batchelor et al.,[61] expanding on previous work by Moakher,[62] used similar theoretical results to define a distance between tensors, obtain their mean and interpolate them. In addition, a new definition of anisotropy called geodesic anisotropy (GA) was introduced, which appeared to be more sensitive to small eigenvalues. Pennec et al. also leveraged this Lie group perspective and developed a computational framework to DT processing with a particular emphasis on interpolation, regularization and restoration of noisy tensor fields.[63] Finally, Lenglet et al.[64] relied on the information geometry of the space of multivariate normal distributions with zero mean to tackle similar theoretical questions, while focusing on the estimation and level-set-based segmentation[65] of DTI data. A related and recent work, which focuses on the DT estimation problem,[66] formulates a Bayesian framework for the simultaneous estimation and regularization of DTI data, while accounting for Rician noise in diffusion-weighted data and providing error bounds. The geodesic distance between two DTs, common to all these studies, is defined as

$$d(D_1, D_2) = \sqrt{tr\left(\log^2\left(D_1^{-1}D_2\right)\right)} \tag{5}$$

This affine-invariant metric prevents the generation of non-positive DTs and limits the 'swelling' effect known to increase eigenvalues disproportionally and affect diffusivity and anisotropy estimates. However, one of the drawbacks of these approaches is their relatively high computational requirement due to matrix operations and the need for optimization methods, since closed-form expressions do not exist in many cases. To address this situation, Arsigny et al. introduced the *log-Euclidean* framework[67,68] and applied it to data interpolation and regularization. Under this framework, Riemmanian operations are converted to Euclidean ones by transforming DTs into their matrix logarithms (which are symmetric matrices). The key finding of this work was that, thanks to one-to-one correspondences via the matrix logarithm and exponential, tensors can be treated as vectors, thereby simplifying and speeding up computations. Equation 5 becomes

$$d(D_1, D_2) = \|\log(D_1) - \log(D_2)\|$$

but it should be noted that affine invariance is lost and replaced by similarity invariance. A comparison of these metrics, along with the introduction of a new Procrustes size-and-shape metric, with its origin in shape statistics, was recently proposed by Dryden et al.[69]

Although scalar-based (fractional anisotropy, diffusivity, etc.) analyses still largely dominate when it comes to clinical or neuroscience applications, investigators have started to adopt these new developments, e.g. to process clinical data with low SNR[70] and perform statistical analyses[71] to detect white-matter lesions in patients with multiple sclerosis. However, despite their ability to enforce physically meaningful constraints, affine- or similarity-invariant metrics have been shown potentially to bias the analysis of normally distributed DT data,[72] therefore requiring investigators to select the metric carefully in light of their particular application.

Recent works have focused on multivariate parametric and non-parametric tests, as well as hypothesis-testing procedures for DT data, and have investigated the relevance and impact of non-Euclidean metrics.[73-75] For instance, in Lee et al.,[73] a Hotelling's T^2 test applied to log-Euclidean transformed DT data was shown to outperform univariate analysis of DT-derived scalar measures. Again, careful considerations appear to be necessary for such parametric tests, which assume multivariate normality of DTs and their interaction with non-Euclidean metrics.[72,76] Using affine- or similarity-invariant metrics in combination with permutation-based[76,77] or Cramer[76] tests also did not appear to improve the performance of these non-parametric tests. However, using the Cholesky decomposition of DTs, as introduced in Wang et al.,[78] it was demonstrated that,[79,80] in addition

to decreased computational time, a non-parametric two-sample test can detect differences in a specific brain region between young children with dyslexia and controls.

3.2 | Orientation distribution functions

Generalizing the concepts, which we briefly outlined in the previous section, to orientation distribution functions derived from high angular resolution diffusion imaging is challenging, in part because of the multi-directional nature of ODFs. This can lead to the mixing or generation of erroneous fiber orientations when performing simple operations such as averaging.[81] ODFs are symmetric spherical probability density functions commonly approximated using the spherical harmonic basis,[82] although other approximation methods, using e.g. mixtures of von Mises–Fisher distributions[83] or spherical ridgelets,[84] have also been proposed. The primary application of such approximation methods has been the accurate estimation and characterization of ODFs to extract white-matter fiber orientations (e.g. for tractography). Defining metrics between ODFs for interpolation[85] or segmentation purposes[86] can easily be done by using the Euclidean distance between spherical harmonic coefficients,[86] although this does not account for the intrinsic properties of the (Riemannian) space of ODFs. Chiang et al.[85] first introduced the idea of using the Fisher–Rao Riemannian metric to compare ODFs. In particular, they used this idea to perform spatial interpolation of ODFs and study genetic influences on white-matter fiber organization. This metric had been introduced in the computer vision literature[87] and provides closed-form expressions for geodesic distance, as well as exponential and logarithm maps. Considering the space of spherical probability density functions $\{p : \mathbb{S}^2 \mapsto \mathbb{R}^+ | \int_{\mathbb{S}^2} p(s)\ \mathrm{d}s = 1\}$, the space of square-root representations $\psi(s) = \sqrt{p(s)}$ is the Hilbert unit sphere, where the Fisher–Rao metric becomes the standard $\mathbb{L}^2$ metric. It can be shown, for instance, that the geodesic distance is defined as

$$d(\psi_1, \psi_2) = \cos^{-1}\left(\int_{\mathbb{S}^2} \psi_1(s)\psi_2(s)\ \mathrm{d}s\right)$$

This was used by Cheng et al.[88] and Goh et al.[89,90] to propose frameworks for computational and statistical analysis of ODF data. While Cheng et al. focused on the estimation and interpolation of ODFs, Goh et al. developed tools for the anisotropic filtering and statistical analysis of ODFs. They proposed applying the concept of principal geodesic analysis[91] to ODFs, to study the modes of variation of a set of ODFs, and they generalized the Hotelling's T^2 statistic for performing multivariate hypothesis testing on two populations of ODFs. This was applied to detect asymmetries of the white matter and led to the identification of significant clusters in the language and sensorimotor areas, for which the Riemannian metric appeared to be more sensitive than the Euclidean metric. Related work leveraging the properties of the Fisher–Rao metric in a sparse Riemannian spectral clustering framework also demonstrated the possibility of extracting fiber pathways reliably in complex white matter areas.[92]

Finally, recent contributions have aimed to design metrics producing more physically meaningful results, as they relate to the shape of ODFs. For instance, it has been demonstrated that interpolating single-fiber ODFs with peaks at different locations, using the Fisher–Rao metric, can result in two-fiber ODFs. To alleviate such issues, one can separate the orientation and shape information contained in an ODF, thereby defining a product space in which orientation and shape are independently compared and new statistics can be defined.[93] Similar ideas were pursued[81] by introducing a group-action-induced distance.

We have summarized *some* of the recent efforts to define metrics for DTs and ODFs, which respect their inherent mathematical properties, with a particular emphasis on statistical analysis. It appears important to move beyond the scalar (e.g. fractional anisotropy, diffusivity) parametric or non-parametric population studies, in order better to leverage the great amount of information encoded in these local models of diffusion. Nonetheless, as we have outlined, care must be taken in doing so, as significant bias can be introduced when these metrics do not account for the proper distributions or noise models. However, it seems apparent that, at least for ODFs, recent works can enforce both mathematically and physically meaningful constraints, which may ultimately prove useful in statistical analysis of these data for neuroscience and clinical studies.

4 | REGISTRATION METHODS FOR DIFFUSION MRI

Registration is a key tool in medical imaging, with applications from population studies to surgical planning. Given two objects I and J, the registration problem is that of finding a transformation ϕ that, when applied to the object J, makes it 'look' as close to I as possible. The registration problem is usually formulated as the minimization problem

$$\arg\min_{\phi \in \Phi} \mathcal{M}(I, \phi^* J) + \mathcal{R}(\phi) \tag{6}$$

Equation 6 aims to find the transformation ϕ from the set of transformations Φ that minimizes the dissimilarity measure $\mathcal{M}$ between I and $\phi^* J$. Throughout this article, $\phi^* J$ represents J deformed according to the transformation ϕ. We prefer this notation to the less general composition rule $J \circ \phi$, as these deformations have different mathematical interpretations depending on whether J is a scalar image, a diffusion-weighted image or a three-dimensional object such as a white-matter tract. Furthermore, to reduce the possible space of solutions, hypotheses on ϕ such as the regularity are represented by the term $\mathcal{R}(\phi)$.

Finding the optimal deformation ϕ, which is usually either a linear transformation or a deformable one, by minimizing Equation 6 has three main points that must be specifically addressed in the dMRI case.

1. How to quantify the difference between two elements representing or computed from diffusivity, specifically the formulation of $\mathcal{M}(\cdot,\cdot)$
2. How the diffusivity information or its derivatives such as tracts must be warped; specifically, how $\phi^* J$ is formulated and implemented.
3. How to incorporate the previous two points into the minimization scheme in Equation 6.

In the remainder of this section, we focus on the different approaches to the aforementioned items and we refer the reader interested in the deformation space Φ, the regularization term $\mathcal{R}(\phi)$ and the overall optimization schemes to existing reviews on this topic.[94]

4.1 | Image-based registration

In the case where I and J are images, they are commonly viewed as spatial functions $I, J : \mathbb{R}^3 \mapsto \mathbb{I}$. In this formulation, $\mathbb{I}$ can denote a subset of real numbers $\mathbb{I} \subseteq \mathbb{R}$ for scalar image registration, a subset of 3×3 positive-definite matrices $\mathbb{I} \subseteq \mathbb{S}^3_+$ in the case of DTI, and, more generally, a subset of spherical $\mathbb{I} \subseteq (S^2 \mapsto \mathbb{R})$ for HARDI or three-dimensional functions $\mathbb{I} \subseteq (\mathbb{R}^3 \mapsto \mathbb{R})$ for multi-shell or DSI approaches. In the scalar case, the application of the transformation ϕ to the image J takes the form

$$(\phi^* J)(x) = J(\phi(x)) \tag{7}$$

However, in cases where the images are vector fields, tensor fields or more complex representations of the dMRI signal, an extra transformation is required. We have illustrated the need for this transformation in Figure 3. Applying the transformation ϕ to the image J can then be divided into two steps.

1. Obtain the diffusivity information $N \in \mathbb{I}$ of the warped image $\phi^* J$ at x:

$$N = J(\phi(x)) \tag{8}$$

2. Warp the diffusivity information N according to the deformation ϕ:

$$\phi^* N = \text{warp}(N, D_x \phi) \tag{9}$$

In accordance with the formalization of Cao et al.,[95] these two steps represent the action of ϕ on tensor fields. Specifically, the first step is the change of coordinates, while the second, which depends on $D_x\phi$, the Jacobian of ϕ at x, accounts for reorientation and, if needed, scaling.

Much of the effort in dMRI registration is focused on the warp in Equation 9. This presents two important computational challenges: first, registration algorithms have to devise a warp operator for the diffusivity data; second, the algorithms must incorporate the warp in the optimization process.

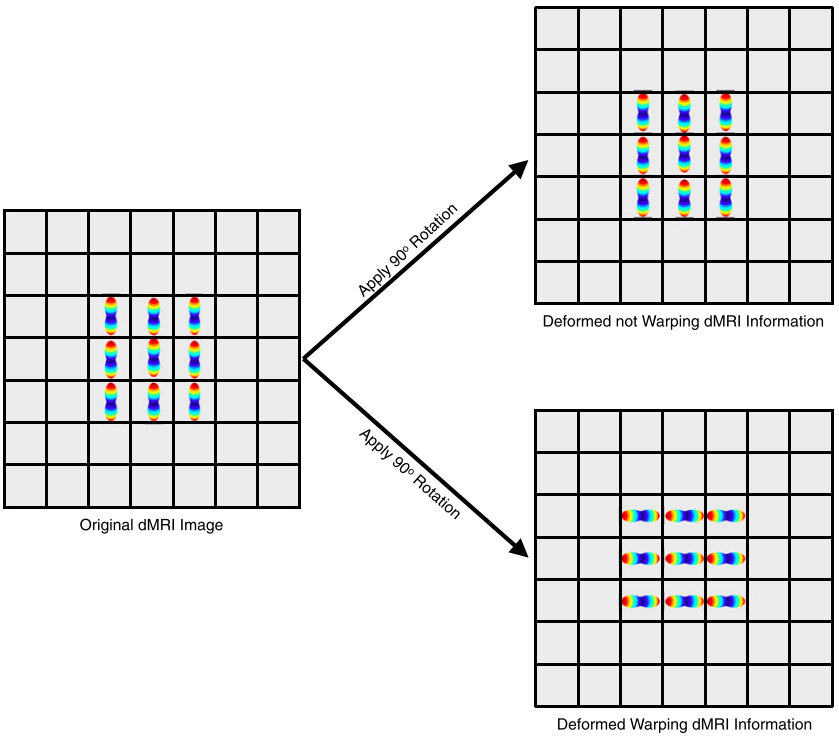

FIGURE 3 Two rotation transformations applied to the dMRI field on the left. The one on the top right does not include the warping of diffusivity information; the one on the bottom right does

The most common approach in statistical analyses of dMRI images is still to choose a scalar measure derived from a dMRI acquisition and perform registration on that scalar image.[96] However, these techniques drive registrations according to a sub-optimal subset of the information contained in a dMRI image. To address this problem, Alexander et al.[97] studied approaches for diffusion tensor (DT) registration. They compared using a combination of scalar measures versus taking the Frobenius norm between tensors, while testing different methodologies to warp the diffusion information. They showed that, for most DT applications, quantifying the image difference using full tensor information and warping by reorienting the tensors yielded an improved registration result. This first step in dMRI image registration created a lasting framework for diffusivity information warping and left two problems open: first, the DT warping was performed in an alternate optimization scheme, leading to instability in the solutions; second, the proposed framework was hard to extend to the novel trend of diffeomorphic optimization techniques, which was achieving more stable results in scalar registration and template estimation.[98,99]

The results produced by Alexander et al.[97] opened a new research trend: the exploration of similarity measures for DT images. Ruiz-Alzola et al.[100] proposed a generalization of the cross-correlation metric for scalar images to the tensor space. Their work was more robust to noise than that of Alexander et al[97] However, incorporating the DT rotation into the optimization framework proved to be a difficult task. To decrease the computational costs of deformable registration, Park et al.[101] proposed to frame the problem in terms of the multichannel Demons algorithm[102] using a vector with components including the T_2 image obtained by setting the b-value to 0 s/mm^2 in the dMRI and scalar measures derived from DT images, as well as components of the DT. Although this made the registration much faster and reduced memory consumption, it added the non-trivial problem of how to weight the different channels. Additional multi-channel approaches explored the use of mutual information as a metric to perform affine and non-rigid registration using DTI or DWI images,[103,104] with tensor reorientation in the case of DTI images. Up to this point, registration techniques had begun to agree on the idea of using the Frobenius norm for tensors. Being able to perform deformable diffeomorphic registration and template estimation of dMRI images was, nonetheless, still an open problem.

Zhang et al.[105] proposed a diffeomorphic registration algorithm and deformable template estimation using the Euclidean norm between the deviatoric tensor of a DT as a metric and parameterizing the deformation field as a multi-scale patchwork of affine deformations. This parameterization is invertible, greatly improving the template estimation process. Within this framework, the gradient of the registration cost function, shown in Equation 6, can be computed analytically, enabling the use of a large number of efficient optimization strategies to register the images. Previous registration approaches had not produced an analytic gradient for the registration cost function, instead implementing it thorough numerical or heuristic approaches, resulting in algorithms with reduced numerical stability. Soon after, Cao et al.[106] used the Frobenius norm and a clever formulation of the preservation of principal direction (PPD)[97] warping technique to formulate the problem within the large deformation diffeomorphic metric mapping (LDDMM) framework,[107] which most commonly uses the Euclidean metric between image elements. Both approaches were stable and suitable for generating dMRI templates, while the Zhang et al.[105] approach required less computation time. Later, Yeo et al.[108] took this a step further, deriving a general framework for incorporating the gradient of the DT warp, shown in Equation 9, into a larger set of registration techniques. This enabled them to produce a diffeomorphic Demons algorithm for DT registration and compare different similarity metrics for tensor fields.

As more advanced acquisition techniques for dMRI became common,[109,110] registration approaches were extended and adapted. In these approaches, the diffusivity M at each point of the images was now a spherical function, such as the ODF,[109] or a three-dimensional function, such as raw DSI information.[110] Goh et al.[111] addressed the ODF case by first devising a Riemmanian space to embed these functions and then deriving a diffeomorphic registration algorithm.Hsu et al.[112,113] addressed the DSI case by registering the image in the full six-dimensional space (three spatial dimensions + three dimensions indicating a 3D vector in diffusion space). On the other hand, Zhang et al.[114] opted for a more general approach. Their work aimed to register the raw DWI images using the LDDMM framework while reorienting and resampling the spherical functions at each voxel to match the acquisition scheme.[115]

4.2 | White matter tract-based approaches

An alternative to image-based registration is to perform registration on the white matter tracts directly.[19] Note that image registration techniques act on the spatial domain of the diffusion image, while tracts are usually defined as curves on the image's co-domain. Hence, to register tracts while keeping the parameterization of deformations consistent with image-based registration, the deformation needs to be applied on the co-domain of the diffusion image. In practice, the tracts must be deformed in the opposite direction from the images (i.e. by applying the forward transformation to the tract points, rather than the inverse or image resampling transformation). An example of this is the application of a deformation to a single point in the co-domain of an image: given an image consisting of a dimensionless point at coordinate c, $J(x) = \delta(c - x)$, applying the deformation ϕ to the domain of J is equivalent to applying ϕ^{-1} to the coordinate c, which is defined on J's co-domain. More formally,

$$\phi^* J = J(\phi(x)) = \delta(c - \phi(x)) = \delta(\phi^{-1}(c) - x) \tag{10}$$

The first proposed tract registration approach performed rigid registration of whole-brain fiber tracts by first finding the best matched pairs of fibers across the two datasets, then estimating a local transformation using points from each fiber pair, and finally computing an overall global transform.[116] This process was repeated in an iterative multiscale fashion. To perform population statistics on tracts, Corouge et al.[117] proposed a framework to register groups of tracts using linear transformations. This technique represented tracts as sequences of N points and used a Euclidean distance between these matrices of $\mathbb{R}^{N\times 3}$. This representation imposes two artefacts on the tracts: an orientation and a fixed discrete

length. To address this, the approach of Corouge et al. required a careful reparameterization of the tracts to have the same length and orientation. Ziyan et al.[118,119] produced a deformable registration for tracts. They achieved this by representing the tracts as images of point density in space and quantifying the similarity between tracts through well-known measures of density agreement. This representation enabled them to remove the requirement of a point-to-point correspondence and equivalent parameterization of white matter tracts. Durrleman et al.[120] took this a step further by representing the tracts as dense vector fields and implementing an LDDMM registration algorithm. Their approach used the current mathematical framework to take the orientation of the tracts explicitly into account and enable sparse representation to reduce computation time. The main drawback of this approach was due to the formalization of tracts as oriented parametric curves. Consequently, their approach needs a coherent tract orientation: two otherwise identical tracts, but with opposite orientations, will be considered infinitely different. Then, Wassermann et al.[121] combined the two approaches based on density representations of tracts[118,120] to produce a diffeomorphic tract registration and template estimation algorithm that did not require consistent orientation. Finally, two recent approaches produced efficient tract-based unbiased template estimations[122] and statistical analyses[123] based on explicit tract parameterizations.

4.3 | Computational costs

For dMRI image registration algorithms, once the registration algorithm and the representation of the deformation are fixed, the computational cost increases with the dimensionality of the representation of diffusion information. This is due to the computation of the metric, which usually increases at most quadratically with the diffusion representation,[108] but in general increases linearly with the number of components.[105,111,113] Moreover, a more costly increment to the computational cost is the warp strategy, shown in Equation 9, which is at least quadratic with respect to the dimensionality of the diffusion information,[97] but can be much higher when diffusion information is non-parametric.[115] Overall, the computational cost of dMRI registration depends on both the metric and warping operations needed for dMRI registration.

In the case of tract-based registration algorithms, the cost can be divided into two trends: techniques working directly on tracts,[122,123] the computational cost of which depends directly on the number of tracts and the number of points representing each tract, and those representing tract bundles as spatial functions, the cost of which is equivalent to registering a scalar or vector image.[118,120,121] In general, if the number of tracts registered is large, e.g. a full-brain tractography of a hemisphere, the run time is at least as long as that of full dMRI image registration. However, if it is not large, e.g. the registration is aimed at a specific bundle, the run time will be lower than that of dMRI image registration techniques.

5 | FUTURE DIRECTIONS IN COMPUTATIONAL DMRI

Today, there are many possible dMRI acquisition and analysis strategies for neuroimaging research. The choice of methods may depend on the neuroscientific or clinical question of interest, the constraints for acquisition and computational processing time and the researchers' awareness of potential pitfalls. There are still many open challenges in dMRI, including non-specificity of traditional DTI-derived measurements,[124,125] uncertain anatomical accuracy of dMRI tractography[126-128] and a general lack of ground truth, which is partially addressed using synthetic or physical fiber phantoms.[129,130] These challenges are expected to inspire future developments in computational dMRI.

Quantitative and anatomical validation is becoming an important aspect of computational dMRI. The dMRI analysis field is developing a strong track record of community validation challenges at the Medical Image Computing and Computer Assisted Intervention (MICCAI), International Society for Magnetic Resonance in Medicine (ISMRM) and International Symposium on Biomedical Imaging (ISBI) conferences,[†] including challenges in tractography in phantoms,[129,131] tractography in clinical cases[132] and model reconstruction.[133,134] The clinical community is becoming increasingly aware that multi-fiber models beyond the diffusion tensor can improve anatomical accuracy of tractography,[11,135-142] and there is increasing development of open-source dMRI software that moves beyond the diffusion tensor.[10,14,143-148]

'Big data' is another important direction for future developments in computational dMRI. Large open datasets, such as the Human Connectome Project[12] and the UK Biobank,[149] are being acquired and released to enable the study of multimodal imaging, genetics and bioinformatics data. To handle big data, future computational dMRI algorithms are expected to require improvements in speed, memory usage and the ability to correlate dMRI information with other multimodal data. Another research direction is to synthesize large dMRI datasets by statistically harmonizing multiple smaller datasets[150] to reduce across-site variability of measures such as fractional anisotropy.[151]

The advances described in this article represent crucial steps forward for dMRI computational analysis. However, important basic research is under way that may change our assumptions about the brain's microstructure and connectivity: current theories about the organization of axons into sheets[152-155] and the possibility that axons take sharp turns or branch at 90 degrees throughout the brain[156] have important implications for the future of tractography methods and microstructure models. In fact, the true three-dimensional morphology of neurons is not yet known and it is currently an active field of study.[157] In the future, more detailed microstructural and neuroanatomical information may become available using advanced 'multi-dimensional' dMRI acquisitions that employ diffusion-sensitizing magnetic field gradients in sophisticated ways.[158,159] Such novel dMRI acquisitions will require future advances in mathematical modeling and computational analysis.

[†]Some recent challenges are yet unpublished, including http://hardi.epfl.ch/static/events/2013_ISBI/, http://tractometer.org/ismrm_2015_challenge/ and http://cmic.cs.ucl.ac.uk/wmmchallenge/

6 | CONCLUSION

Thus far, standard DTI-based computational methods, which have been available since the mid-1990s, have had a large impact in scientific research.[160] More recently, significant progress has been made with HARDI, multishell, q-ball and DSI imaging.[161] However, there is still a need for methods that can measure and model the brain's true underlying tissue geometry and biophysical parameters. Based on the current progress in validating advanced methods and the expected future increases in computational power, we look forward to an increasingly successful application of advances in computational and statistical dMRI to neuroimaging research.

ACKNOWLEDGEMENTS

We gratefully acknowledge the following sources of funding: NIH P41 EB015894, R01 EB008432, U01 CA199459, R03 NS088301, P41 EB015898, P41 EB015902, and R01 MH074794. This work is also supported by the Center for Biomedical Imaging (CIBM) of the Geneva-Lausanne Universities and the EPFL, as well as the foundations Leenaards and Louis-Jeantet.

ORCID

Lauren J. O'Donnell http://orcid.org/0000-0003-0197-7801
Alessandro Daducci http://orcid.org/0000-0002-4677-6678
Demian Wassermann http://orcid.org/0000-0001-5194-6056
Christophe Lenglet http://orcid.org/0000-0003-4646-3185

REFERENCES

1. Basser P. Historical perspectives and future outlook of diffusion MRI. *NMR Biomed*. Submitted.
2. Assaf F, Johansen - Berg H, Thiebaut de Schotten M. The role of diffusion MRI in neuroscience. *NMR Biomed*. 2017;e3762. https://doi.org/10.1002/nbm.3762
3. Jbabdi S, Sotiropoulos SN, Haber SN, Van Essen DC, Behrens TE. Measuring macroscopic brain connections in vivo. *Nat Neurosci*. 2015;18(11):1546-1555.
4. Bastiani M, Roebroeck A. Unraveling the multiscale structural organization and connectivity of the human brain: the role of diffusion MRI. *Front Neuroanat*. 2015;9:77.
5. Mueller BA, Lim KO, Hemmy L, Camchong J. Diffusion MRI and its role in neuropsychology. *Neuropsychol Rev*. 2015;25(3):250-271.
6. Delouche A, Attyé A, Heck O, et al. Diffusion MRI: Pitfalls, literature review and future directions of research in mild traumatic brain injury. *Eur J Radiol*. 2016;85(1):25-30.
7. Abhinav K, Yeh FC, Pathak S, et al. Advanced diffusion MRI fiber tracking in neurosurgical and neurodegenerative disorders and neuroanatomical studies: A review. *Biochim Biophys Acta (BBA) – Mol Basis Disease*. 2014;1842(11):2286-2297.
8. Calabrese E. Diffusion tractography in deep brain stimulation surgery: A review. *Front Neuroanat*. 2016;10:45.
9. O'Donnell LJ, Westin CF. An introduction to diffusion tensor image analysis. *Neurosurg Clin North Am*. 2011;22(2):185]-196.
10. Malcolm JG, Shenton ME, Rathi Y. Filtered multitensor tractography. *IEEE Trans Med Imaging*. 2010;29(9):1664-1675.
11. Chen Z, Tie Y, Olubiyi O, et al. Reconstruction of the arcuate fasciculus for surgical planning in the setting of peritumoral edema using two-tensor unscented Kalman filter tractography. *NeuroImage: Clin*. 2015;7:815-822.
12. Van Essen DC, Smith SM, Barch DM, et al. The WU-Minn human connectome project: an overview. *Neuroimage*. 2013;80:62-79.
13. Talos IF, O'Donnell L, Westin CF, et al. Diffusion tensor and functional MRI fusion with anatomical MRI for image-guided neurosurgery. *International Conference on Medical Image Computing and Computer-Assisted Intervention*. Montreal: Springer; 2003:407-415.
14. Fedorov A, Beichel R, Kalpathy-Cramer J, et al. 3D Slicer as an image computing platform for the Quantitative Imaging Network. *Magn Reson Imaging*. 2012;30(9):1323-1341.
15. Basser PJ, Mattiello J, LeBihan D. MR diffusion tensor spectroscopy and imaging. *Biophys J*. 1994;66(1):259-267.
16. O'Donnell LJ, Golby AJ, Westin CF. Fiber clustering versus the parcellation-based connectome. *NeuroImage*. 2013;80:283-289.
17. Hagmann P. From diffusion MRI to brain connectomics. *PhD thesis*. Lausanne: École Polytechnique Fédérale de Lausanne; 2005.
18. Sotiropoulos SN, Zalesky A. Building connectomes using diffusion MRI: why, how and but. *NMR Biomed*. 2017;e3752. https://doi.org/10.1002/nbm.3752
19. Jeurissen B, Descoteaux M, Mori S, Leemans A. Diffusion MRI fiber tractography of the brain. *NMR Biomed*. 2017;e3785. https://doi.org/10.1002/nbm.3785
20. Jones D. Challenges and limitations of quantifying brain connectivity in vivo with diffusion MRI. *Imaging Med*. 2010;2(3):341-55.
21. Jbabdi S, Johansen-Berg H. Tractography: where do we go from here?. *Brain Connect*. 2011;1(3):169-83.
22. Conturo TE, Lori NF, Cull TS, et al. Tracking neuronal fiber pathways in the living human brain. *Proc Natl Acad Sci USA*. 1999;96(18):10422-7.
23. Mori S, Crain B, Chacko V, van Zijl PCM. Three-dimensional tracking of axonal projections in the brain by magnetic resonance imaging. *Ann Neurol*. 1999;45(2):265-9.
24. Jones D, Knösche T, Turner R. White matter integrity, fiber count, and other fallacies: the do's and don'ts of diffusion MRI. *NeuroImage*. 2013;73:239-54.

25. Parker G, Haroon H, Wheeler-Kingshott C. A framework for a streamline-based probabilistic index of connectivity (PICo) using a structural interpretation of MRI diffusion measurements. *J Magn Reson Imaging*. 2003;18:242-54.
26. Behrens T, Woolrich M, Jenkinson M, et al. Characterization and propagation of uncertainty in diffusion-weighted MR imaging. *Magn Reson Med*. 2003;50:1077-88.
27. Kreher BW, Mader I, Kiselev VG. Gibbs tracking: a novel approach for the reconstruction of neuronal pathways. *Magn Reson Med*. 2008;60(4):953-963.
28. Fillard P, Poupon C, Mangin JF. A novel global tractography algorithm based on an adaptive spin glass model. In: Proc. MICCAI, London; 2009:927-34.
29. Reisert M, Mader I, Anastasopoulos C, Weigel M, Schnell S, Kiselev V. Global fiber reconstruction becomes practical. *Neuroimage*. 2011;54(2):955-62.
30. Sherbondy A, Dougherty R, Ananthanarayanan R, Modha D, Wandell B. Think global, act local; projectome estimation with BlueMatter. In: Proc. MICCAI, London; 2009:861-8.
31. Smith RE, Tournier JD, Calamante F, Connelly A. SIFT: spherical-deconvolution informed filtering of tractograms. *Neuroimage*. 2013;67:298-312.
32. Tournier JD, Calamante F, Connelly A. Robust determination of the fibre orientation distribution in diffusion MRI: non-negativity constrained super-resolved spherical deconvolution. *NeuroImage*. 2007;35:1459-72.
33. Smith RE, Tournier JD, Calamante F, Connelly A. SIFT2: Enabling dense quantitative assessment of brain white matter connectivity using streamlines tractography. *NeuroImage*. 2015;119:338-51.
34. Smith RE, Tournier JD, Calamante F, Connelly A. The effects of SIFT on the reproducibility and biological accuracy of the structural connectome. *NeuroImage*. 2015;104:253-65.
35. Yeh CH, Smith RE, Liang X, Calamante F, Connelly A. Correction for diffusion MRI fibre tracking biases: The consequences for structural connectomic metrics. *NeuroImage*. 2016;142:150-62.
36. Sherbondy A, Rowe M, Alexander D. MicroTrack: An Algorithm for Concurrent Projectome and Microstructure Estimation. In: Proc. MICCAI, Beijing; 2010:183-90.
37. Alexander D, Hubbard P, Hall M, et al. Orientationally invariant indices of axon diameter and density from diffusion MRI. *NeuroImage*. 2010;52(4):1374-89.
38. Reddy CP, Rathi Y. Joint multi-fiber NODDI parameter estimation and tractography using the unscented information filter. *Front Neurosci*. 2016;10:166.
39. Zhang H, Schneider T, Wheeler-Kingshott CA, Alexander DC. NODDI: Practical in vivo neurite orientation dispersion and density imaging of the human brain. *NeuroImage*. 2012;61:1000-16.
40. Girard G, Fick R, Descoteaux M, Deriche R, Wassermann D. AxTract: Microstructure-driven tractography based on the ensemble average propagator. In: Proc. IPMI, Isle of Skye; 2015:675-86.
41. Daducci A, Canales-Rodriguez E, Zhang H, Dyrby T, Alexander D, Thiran JP. Accelerated microstructure imaging via convex optimization (AMICO) from diffusion MRI data. *Neuroimage*. 2015;105:32-44.
42. Daducci A, Dal Palú A, Lemkaddem A, Thiran JP. A convex optimization framework for global tractography. In: Proc. IEEE ISBI, San Francisco; 2013:524-7.
43. Daducci A, Dal Palú A, Lemkaddem A, Thiran JP. COMMIT: Convex optimization modeling for microstructure informed tractography. *IEEE Trans Med Imaging*. 2014;33(1):246-57.
44. Panagiotaki E, Schneider T, Siow B, Hall MG, Lythgoe MF, Alexander DC. Compartment models of the diffusion MR signal in brain white matter: a taxonomy and comparison. *NeuroImage*. 2012;59(3):2241-54.
45. Pestilli F, Yeatman J, Rokem A, Kay K, Wandell B. Evaluation and statistical inference for human connectomes. *Nat Methods*. 2014;11:1058-63.
46. Daducci A, Dal Palú A, Descoteaux M, Thiran JP. Microstructure informed tractography: pitfalls and open challenges. *Front Neurosci*. 2016;10:247.
47. Lebel C, Treit S, Beaulieu C,. A review of diffusion MRI of typical white matter development from early childhood to young adulthood. *NMR Biomed*. 2017;e3778. https://doi.org/10.1002/nbm.3778
48. Cercignani M, Wheeler-Kingshott C. From micro- to macro-structures in multiple sclerosis: what can we learn from diffusion imaging. *NMR Biomed*. Submitted.
49. Catani M, Hess C, Stieltjes B. Diffusion MRI in clinical practice, *NMR Biomed*. Submitted.
50. Novikov DS, Jespersen SN, Kiselev VG, Fieremans E. Quantifying brain microstructure with diffusion MRI: Theory and parameter estimation. *NMR Biomed*. Submitted.
51. Alexander DC, Dyrby TB, Nilsson M, Zhang H. Imaging brain microstructure with diffusion MRI: Practicality and applications. *NMR Biomed*. Submitted.
52. Dell'Acqua F, Tournier JD. Modelling White Matter with Spherical Deconvolution: How and Why? *NMR Biomed*. Submitted.
53. Mahalanobis PC. On the generalized distance in statistics. *Proc Natl Inst Sci (Calcutta)*. 1936;2:49-55.
54. Rao R. Information and the accuracy attainable in the estimation of statistical parameters. *Bull Calcutta Math Soc*. 1945;37:81-91.
55. Peter A, Rangarajan A. Shape analysis using the Fisher–Rao R. metric: unifying shape representation and deformation. In: Biomedical Imaging: Nano to Macro, 2006. 3rd IEEE International Symposium, Arlington; 2006:1164-1167.
56. Amari SI. *Differential-Geometrical Methods in Statistics*, (Lecture Notes in Statistics 28). New York: Springer; 1985.
57. Madsen L. The geometry of statistical models. PhD thesis, University of Copenhagen; 1978.
58. Pajevic S, Basser PJ. Parametric and non-parametric statistical analysis of DT-MRI data. *J Magn Reson*. 2003;161(1):1-14.
59. Basser PJ, Pajevic S. A normal distribution for tensor-valued random variables: applications to diffusion tensor MRI. *IEEE Trans Med Imaging*. 2003;22(7):785-94.
60. Fletcher T, Joshi S. Principal geodesic analysis on symmetric spaces: Statistics of diffusion tensors. In: Jan, ed. *Computer Vision and Mathematical Methods in Medical and Biomedical Image Analysis: ECCV 2004 Workshops CVAMIA and MMBIA Prague, Czech Republic, May 15, 2004 Revised Selected Papers*, Vol. 3117. Prague: Springer; 2004:87-98.
61. Batchelor PG, Moakher M, Atkinson D, Calamante F, Connelly A. A rigorous framework for diffusion tensor calculus. *Magn Reson Med*. 2005;53(1):221-5.
62. Moakher M. A differential geometric approach to the geometric mean of symmetric positive-definite matrices. *SIAM J Matrix Anal Appl*. 2005;26(3):735-747.

63. Pennec X, Fillard P, Ayache N. A Riemannian framework for tensor computing. *Int J Comput Vision*. 2006;66(1):41-66.
64. Lenglet C, Rousson M, Deriche R, Faugeras O. Statistics on the manifold of multivariate normal distributions: Theory and application to diffusion tensor MRI processing. *J Math Imaging and Vision*. 2006;25(3):423-444.
65. Lenglet C, Rousson M, Deriche R. DTI segmentation by statistical surface evolution. *IEEE Trans Med Imaging*. 2006;25(6):685-700.
66. Krajsek K, Menzel MI, Scharr H. A Riemannian Bayesian framework for estimating diffusion tensor images. *Int J Comput Vision*. 2016;120(3):272-299.
67. Arsigny V, Fillard P, Pennec X, Ayache N. Log-Euclidean metrics for fast and simple calculus on diffusion tensors. *Magn Reson Med*. 2006;56(2):411-21.
68. Arsigny V, Fillard P, Pennec X, Ayache N. Geometric means in a novel vector space structure on symmetric positive-definite matrices. *SIAM J Matrix Anal Appl*. 2007;29(1):328-347.
69. Dryden IL, Koloydenko A, Zhou D. Non-Euclidean statistics for covariance matrices, with applications to diffusion tensor imaging. *Ann Appl Stat*. 2009;3(3):1102-1123.
70. Fillard P, Pennec X, Arsigny V, Ayache N. Clinical DT-MRI estimation, smoothing, and fiber tracking with log-Euclidean metrics. *IEEE Trans Med Imaging*. 2007;26(11):1472-82.
71. Commowick O, Fillard P, Clatz O, Warfield SK. Detection of DTI white matter abnormalities in multiple sclerosis patients. *Med Image Comput Comput Assist Interv*. 2008;11(1):975-82.
72. Pasternak O, Sochen N, Basser PJ. The effect of metric selection on the analysis of diffusion tensor MRI data. *Neuroimage*. 2010;49(3):2190-204.
73. Lee AD, Lepore N, Lepore F, et al. Brain differences visualized in the blind using tensor manifold statistics and diffusion tensor imaging. In: Frontiers in the Convergence of Bioscience and Information Technologies, 2007. FBIT 2007, Jeju Island; 2007:470-476.
74. Fouque AL, Fillard P, Bargiacchi A, et al. Voxelwise multivariate statistics and brain-wide machine learning using the full diffusion tensor. *Med Image Comput Comput Assist Interv*. 2011;14(2):9-16.
75. Grigis A, Noblet V, Heitz F, et al. Longitudinal change detection in diffusion MRI using multivariate statistical testing on tensors. *Neuroimage*. 2012;60(4):2206-21.
76. Whitcher B, Wisco JJ, Hadjikhani N, Tuch DS. Statistical group comparison of diffusion tensors via multivariate hypothesis testing. *Magn Reson Med*. 2007;57(6):1065-74.
77. Collard A, Phillips C, Sepulchre R. Statistical tests for group comparison of manifold-valued data. In: 52nd IEEE Conference on Decision and Control, Florence; 2013:1144-1149.
78. Wang Z, Vemuri BC, Chen Y, Mareci TH. A constrained variational principle for direct estimation and smoothing of the diffusion tensor field from complex DWI. *IEEE Trans Med Imaging*. 2004;23(8):930-9.
79. Osborne D, Patrangenaru V, Ellingson L, Groisser D, Schwartzman A. Nonparametric two-sample tests on homogeneous Riemannian manifolds, Cholesky decompositions and Diffusion Tensor Image analysis. *J Multivar Anal*. 2013;119:163-175.
80. Ellingson L, Groisser D, Osborne D, Patrangenaru V, Schwartzman A. Nonparametric bootstrap of sample means of positive-definite matrices with an application to diffusion-tensor-imaging data analysis. *Commun Stat – Simul Comput*. 2017;46(6):4851-4879.
81. Cetingul HE, Afsari B, Wright MJ, Thompson PM, Vidal R. Group action induced averaging for HARDI processing. In: Proc IEEE Int Symp Biomed Imaging, Barcelona; 2012:1389-1392.
82. Descoteaux M, Angelino E, Fitzgibbons S, Deriche R. Regularized, fast, and robust analytical q-ball imaging. *Magn Reson Med*. 2007;58(3):497-510.
83. McGraw T, Vemuri BC, Yezierski B, Mareci T. Von Mises–Fisher mixture model of the diffusion ODF. *Proc IEEE Int Symp Biomed Imaging*. 2006;2006:65-68.
84. Michailovich O, Rathi Y. On approximation of orientation distributions by means of spherical ridgelets. *IEEE Trans Image Process*. 2010;19(2):461-77.
85. Chiang MC, Barysheva M, Lee AD, et al. Brain fiber architecture, genetics, and intelligence: a high angular resolution diffusion imaging (HARDI) study. *Med Image Comput Comput Assist Interv*. 2008;11(1):1060-7.
86. Descoteaux M, Deriche R. High angular resolution diffusion MRI segmentation using region-based statistical surface evolution. *J Math Imaging and Vision*. 2009;33(2):239-252.
87. Srivastava A, Jermyn I, Joshi S. Riemannian analysis of probability density functions with applications in vision. In: 2007 IEEE Conference on Computer Vision and Pattern Recognition, Minneapolis; 2007:1-8. ISBN 1063-6919.
88. Cheng J, Ghosh A, Jiang T, Deriche R. A Riemannian framework for orientation distribution function computing. *Med Image Comput Comput Assist Interv*. 2009;12(1):911-8.
89. Goh A, Lenglet C, Thompson PM, Vidal R. A nonparametric Riemannian framework for processing high angular resolution diffusion images (HARDI). In: Computer Vision and Pattern Recognition, 2009. CVPR 2009. IEEE Conference; Miami; 2009:2496-2503. ISBN 1063-6919.
90. Goh A, Lenglet C, Thompson PM, Vidal R. A nonparametric Riemannian framework for processing high angular resolution diffusion images and its applications to ODF-based morphometry. *Neuroimage*. 2011;56(3):1181-201.
91. Fletcher PT, Lu C, Pizer SM, Joshi S. Principal geodesic analysis for the study of nonlinear statistics of shape. *IEEE Trans Med Imaging*. 2004;23(8):995-1005.
92. Cetingul HE, Wright MJ, Thompson PM, Vidal R. Segmentation of high angular resolution diffusion MRI using sparse Riemannian manifold clustering. *IEEE Trans Med Imaging*. 2014;33(2):301-17.
93. Ncube S, Srivastava A. A novel Riemannian metric for analyzing HARDI data. *Proc SPIE*. 2011;7962:79620Q-79620Q–7.
94. Sotiras A, Davatzikos C. Deformable medical image registration: A survey. *IEEE Trans Med Imaging*. 2013;32(7):1153-1190.
95. Cao Y, Miller M, Winslow RL, Younes L. Large deformation diffeomorphic metric mapping of vector fields. *IEEE Trans Med Imaging*. 2005;24(9):1216-1230.
96. Smith SM, Jenkinson M, Johansen Berg H, et al. Tract-based spatial statistics: voxelwise analysis of multi-subject diffusion data. *NeuroImage*. 2006;31(4):1487-1505.
97. Alexander DC, Pierpaoli C, Basser PJ, Gee JC. Spatial transformations of diffusion tensor magnetic resonance images. *IEEE Trans Med Imaging*. 2001;20(11):1131-1139.

98. Christensen G, Johnson HJ. Consistent image registration. *IEEE Trans Med Imaging*. 2001;20(7):568-582.
99. Dupuis P, Grenander U. Variational problems on flows of diffeomorphisms for image matching. *Q Appl Math*. 1998;LVI(3):587-600.
100. Ruiz-Alzola J, Westin CF, Warfield SK, Alberola C, Maier SE, Kikinis R. Nonrigid registration of 3D tensor medical data. *Med Image Anal*. 2002;6(2):143-161.
101. Park HJ, Kubicki M, Shenton ME, et al. Spatial normalization of diffusion tensor MRI using multiple channels. *NeuroImage*. 2003;20(4):1995-2009.
102. Guimond A, Roche A, Ayache N, Meunier J. Three-dimensional multimodal brain warping using the Demons algorithm and adaptive intensity corrections. *IEEE Trans Med Imaging*. 2001;20(1):58-69.
103. Leemans A, Sijbers J, De Backer S, Vandervliet E, Parizel PM. Affine coregistration of diffusion tensor magnetic resonance images using mutual information. *ACIVS*. Antwerp: Springer; 2005:523-530.
104. Van Hecke W, Leemans A, D'Agostino E, et al. Nonrigid coregistration of diffusion tensor images using a viscous fluid model and mutual information. *IEEE Trans Med Imaging*. 2007;26(11):1598-1612.
105. Zhang H, Yushkevich P, Alexander DC, Gee JC. Deformable registration of diffusion tensor MR images with explicit orientation optimization. *Med Image Anal*. 2006;10(5):764-785.
106. Cao Y, Miller M, Mori S, Winslow RL, Younes L. Diffeomorphic matching of diffusion tensor images. In: Conference on Computer Vision and Pattern Recognition Workshop IEEE; New York; 2006:67.
107. Beg M, Miller M, Trouvé A, Younes L. Computing large deformation metric mappings via geodesic flows of diffeomorphisms. *Int J Comput Vision*. 2005;61(2):139-157.
108. Yeo BTT, Vercauteren T, Fillard P, et al. DT-REFinD: Diffusion tensor registration with exact finite-strain differential. *IEEE Trans Med Imaging*. 2009;28(12):1914-1928.
109. Tuch D, Reese T, Wiegell M, Makris N, Belliveau J, Van Wedeen J. High angular resolution diffusion imaging reveals intravoxel white matter fiber heterogeneity. *Magn Reson Med*. 2002;48(4):577-582.
110. Van Wedeen J, Wang R, Schmahmann JD, et al. Diffusion spectrum magnetic resonance imaging (DSI) tractography of crossing fibers. *NeuroImage*. 2008;41(4):1267-1277.
111. Goh A, Lenglet C, Thompson P, Vidal R. A nonparametric Riemannian framework for processing high angular resolution diffusion images and its applications to ODF-based morphometry. *NeuroImage*. 2011;56(3):1181-1201.
112. Du J, Goh A, Qiu A. Diffeomorphic metric mapping of high angular resolution diffusion imaging based on Riemannian structure of orientation distribution functions. *IEEE Trans Med Imaging*. 2012;31(5):1021-1033.
113. Hsu YC, Hsu CH, Tseng W. A large deformation diffeomorphic metric mapping solution for diffusion spectrum imaging datasets. *NeuroImage*. 2012;63(2):818-834.
114. Zhang P, Niethammer M, Shen D, Yap PT. Large deformation diffeomorphic registration of diffusion-weighted imaging data. *Med Image Anal*. 2014;18(8):1290-1298.
115. Yap PT, Wu G, Zhu H, Lin W, Shen D. F-TIMER: Fast tensor image morphing for elastic registration. *IEEE Trans Med Imaging*. 2010;29(5):1192-1203.
116. Leemans A, Sijbers J, De Backer S, Vandervliet E, Parizel P. Multiscale white matter fiber tract coregistration: A new feature-based approach to align diffusion tensor data. *Magn Reson Med*. 2006;55(6):1414-1423.
117. Corouge I, Fletcher P, Joshi SC, Gouttard S, Gerig G. Fiber tract-oriented statistics for quantitative diffusion tensor MRI analysis. *Magn Reson Med*. 2006;10(5):786-798.
118. Ziyan U, Sabuncu MR, O'Donnell LJ, Westin CF. Nonlinear registration of diffusion MR images based on fiber bundles. *Int Conf Med Image Comput Comput-Assisted Intervention*. 2007;10(1):351-358.
119. Ziyan U, Sabuncu M, Grimson WEL, Westin CF. Consistency clustering: A robust algorithm for group-wise registration, segmentation and automatic atlas construction in diffusion MRI. *Int J Comput Vision*. 2009;85(3):279-290.
120. Durrleman S, Pennec X, Trouvé A, Ayache N. Statistical models of sets of curves and surfaces based on currents. *Med Image Anal*. 2009;13(5):793-808.
121. Wassermann D, Bloy L, Verma R, Deriche R. A Gaussian process based framework for white matter fiber tracts and bundles, applications to fiber clustering. In: IPMI, Williamsburg; 2009:200-214.
122. O'Donnell LJ, Wells III WM, Golby AJ, Westin CF. Unbiased groupwise registration of white matter tractography. *In: International Conference on Medical Image Computing and Computer-Assisted Intervention -MICCAI*. Berlin, Heidelberg: Springer; 2012:123-130.
123. Garyfallidis E, Wassermann D, Descoteaux M. Direct native-space fiber bundle alignment for group comparisons. In: Proceedings of the International Symposium in Magentic Resonance in Medicine; 2014:7796.
124. Jones DK, Knösche TR, Turner R. White matter integrity, fiber count, and other fallacies: the do's and don'ts of diffusion MRI. *Neuroimage*. 2013;73:239-254.
125. O'Donnell LJ, Pasternak O. Does diffusion MRI tell us anything about the white matter? An overview of methods and pitfalls. *Schizophr Res*. 2015;161(1):133-141.
126. Thomas C, Frank QY, Irfanoglu MO, et al. Anatomical accuracy of brain connections derived from diffusion MRI tractography is inherently limited. *Proc Natl Acad Sci*. 2014;111(46):16574-16579.
127. Mandelli ML, Berger MS, Bucci M, Berman JI, Amirbekian B, Henry RG. Quantifying accuracy and precision of diffusion MR tractography of the corticospinal tract in brain tumors: clinical article. *J Neurosurg*. 2014;121(2):349-358.
128. Reveley C, Seth AK, Pierpaoli C, et al. Superficial white matter fiber systems impede detection of long-range cortical connections in diffusion MR tractography. *Proc Natl Acad Sci*. 2015;112(21):E2820-E2828.
129. Fillard P, Descoteaux M, Goh A, et al. Quantitative evaluation of 10 tractography algorithms on a realistic diffusion MR phantom. *Neuroimage*. 2011;56(1):220-234.

130. Neher PF, Laun FB, Stieltjes B, Maier-Hein KH. Fiberfox: facilitating the creation of realistic white matter software phantoms. *Magn Reson Med*. 2014;72(5):1460-1470.
131. Côté MA, Girard G, Boré A, Garyfallidis E, Houde JC, Descoteaux M. Tractometer: towards validation of tractography pipelines. *Med Image Anal*. 2013;17(7):844-857.
132. Pujol S, Wells W, Pierpaoli C, et al. The DTI challenge: toward standardized evaluation of diffusion tensor imaging tractography for neurosurgery. *J Neuroimaging*. 2015;25(6):875-882.
133. Daducci A, Canales-Rodriguez E, Descoteaux M, et al. Quantitative comparison of reconstruction methods for intra-voxel fiber recovery from diffusion MRI. *IEEE Trans Med Imaging*. 2014;99:384-399.
134. Ning L, Laun F, Gur Y, et al. Sparse reconstruction challenge for diffusion MRI: Validation on a physical phantom to determine which acquisition scheme and analysis method to use?. *Med Image Anal*. 2015;26(1):316-331.
135. Qazi AA, Radmanesh A, O'Donnell L, et al. Resolving crossings in the corticospinal tract by two-tensor streamline tractography: method and clinical assessment using fMRI. *NeuroImage*. 2009;47:T98-T106.
136. Kuhnt D, Bauer MH, Egger J, et al. Fiber tractography based on diffusion tensor imaging compared with high-angular-resolution diffusion imaging with compressed sensing: initial experience. *Neurosurg*. 2013;72(0 1):165-175.
137. Farquharson S, Tournier JD, Calamante F, et al. White matter fiber tractography: why we need to move beyond DTI: Clinical article. *J Neurosurg*. 2013;118(6):1367-1377.
138. Nimsky C. Fiber tracking – we should move beyond diffusion tensor imaging. *World Neurosurg*. 2014;82(1):35-36.
139. Mormina E, Longo M, Arrigo A, et al. MRI tractography of corticospinal tract and arcuate fasciculus in high-grade gliomas performed by constrained spherical deconvolution: qualitative and quantitative analysis. *Am J Neuroradiol*. 2015;36(10):1853-1858.
140. Caverzasi E, Hervey-Jumper SL, Jordan KM, et al. Identifying preoperative language tracts and predicting postoperative functional recovery using HARDI q-ball fiber tractography in patients with gliomas. *J Neurosurg*. 2015;125(1):33-45.
141. Chen Z, Tie Y, Olubiyi O, et al. Corticospinal tract modeling for neurosurgical planning by tracking through regions of peritumoral edema and crossing fibers using two-tensor unscented Kalman filter tractography. *Int J Comp Assist Radiol Surg*. 2016;11(8):1475-1486.
142. Essayed WI, Zhang F, Unadkat P, Cosgrove GR, Golby AJ, O'Donnell LJ. White matter tractography for neurosurgical planning: A topography-based review of the current state of the art. *NeuroImage: Clinical*. 2017;15:659-672.
143. Cook P, Bai Y, Nedjati-Gilani S, et al. Camino: open-source diffusion-MRI reconstruction and processing. In: Proceedings of the 14th Scientific Meeting of the International Society for Magnetic Resonance in Medicine, Vol. 2759; 2006:2759; Seattle WA, USA.
144. Fritzsche KH, Neher PF, Reicht I, et al. MITK diffusion imaging. *Methods Inf Med*. 2012;51(5):441-488.
145. Garyfallidis E, Brett M, Amirbekian B, et al. Dipy, a library for the analysis of diffusion MRI data. *Front Neuroinformatics*. 2014;8:8.
146. Christiaens D, Reisert M, Dhollander T, Sunaert S, Suetens P, Maes F. Global tractography of multi-shell diffusion-weighted imaging data using a multi-tissue model. *NeuroImage*. 2015;123:89-101.
147. Yeh FC, Badre D, Verstynen T. Connectometry: A statistical approach harnessing the analytical potential of the local connectome. *NeuroImage*. 2016;125:162-171.
148. Norton I, Essayed WI, Zhang F, et al. SlicerDMRI: Open source diffusion MRI software for brain cancer research. *Cancer Res*. 2017. Accepted article.
149. Sudlow C, Gallacher J, Allen N, et al. UK biobank: an open access resource for identifying the causes of a wide range of complex diseases of middle and old age. *PLoS Med*. 2015;12(3):e1001779.
150. Mirzaalian H, de Pierrefeu A, Savadjiev P, et al. Harmonizing diffusion MRI data across multiple sites and scanners. *In: International Conference on Medical Image Computing and Computer-Assisted Intervention*. Munich: Springer; 2015:12-19.
151. Vollmar C, O'Muircheartaigh J, Barker GJ, et al. Identical, but not the same: intra-site and inter-site reproducibility of fractional anisotropy measures on two 3.0 T scanners. *Neuroimage*. 2010;51(4):1384-1394.
152. Wedeen VJ, Rosene DL, Wang R, et al. The geometric structure of the brain fiber pathways. *Science*. 2012;335(6076):1628-1634.
153. Catani M, Bodi I, Dell'Acqua F. Technical comment on 'the geometric structure of the brain fiber pathways'. *Science*. 2012;337(6102):1605.
154. Tax CM, Haije TD, Fuster A, et al. Sheet probability index (SPI): Characterizing the geometrical organization of the white matter with diffusion MRI. *NeuroImage*. 2016;142:260-279.
155. Tax CM, Westin CF, Haije TD, et al. Quantifying the brain's sheet structure with normalized convolution. *Med Image Anal*. 2017;39:162-177.
156. Wedeen VJ, Rosene DL, Wang R, et al. Response to comment on 'the geometric structure of the brain fiber pathways'. *Sci*. 2012;337(6102):1605-1605.
157. Peng H, Hawrylycz M, Roskams J, et al. BigNeuron: large-scale 3D neuron reconstruction from optical microscopy images. *Neuron*. 2015;87(2):252-256.
158. Shemesh N, Jespersen SN, Alexander DC, et al. Conventions and nomenclature for double diffusion encoding NMR and MRI. *Magn Reson Med*. 2016;75(1):82-87.
159. Westin CF, Knutsson H, Pasternak O, et al. Q-space trajectory imaging for multidimensional diffusion MRI of the human brain. *NeuroImage*. 2016;135:345-362.
160. Le Bihan D, Johansen-Berg H. Diffusion MRI at 25: exploring brain tissue structure and function. *Neuroimage*. 2012;61(2):324-341.
161. Johansen-Berg H, Behrens TE. *Diffusion MRI: From Quantitative Measurement to in Vivo Neuroanatomy*. London: Academic Press; 2013.

How to cite this article: O'Donnell LJ, Daducci A, Wassermann D, Lenglet C. Advances in computational and statistical diffusion MRI. *NMR in Biomedicine*. 2019;32:e3805. https://doi.org/10.1002/nbm.3805